Eur. Phys. J. D (2020) 74: 218
https://doi.org/10.1140/epjd/e2020-10327-9

THE EUROPEAN PHYSICAL JOURNAL D

Regular Article

Non-linear Breit–Wheeler process with linearly polarized beams

Alexander I. Titov[1,a] and Burkhard Kämpfer[2,3]

[1] Bogoliubov Laboratory of Theoretical Physics, JINR, Dubna 141980, Russia
[2] Helmholtz-Zentrum Dresden-Rossendorf, 01314 Dresden, Germany
[3] Institut für Theoretische Physik, TU Dresden, 01062 Dresden, Germany

Received 8 June 2020 / Accepted 18 September 2020
Published online 1 November 2020

Abstract. We study the non-linear Breit–Wheeler process $\vec{\gamma}' + \vec{L} \to e^+ + e^-$ in the interaction of linearly polarized probe photons ($\vec{\gamma}'$) with a linearly polarized laser beam ($\vec{L}$). In particular, we consider the asymmetry of the total cross section and the azimuthal electron distributions when the polarizations of the photon and laser beams in the initial state are mutually perpendicular or parallel. Considering intense laser beams and the strong field asymptotic we explore essentially the multi-photon dynamics. The asymmetry exhibits some non-monotonic behavior depending on initial kinematic conditions; it depends sensitively on the laser pulse duration. Our results provide additional knowledge for studying non-linear multi-photon effects in quantum electrodynamics and may be used in planning experiments in upcoming laser facilities.

1 Introduction

The study of elementary photon–electron interaction processes in strong electromagnetic fields in the laboratory is enabled, to a large extent, by facilities which provide intense and ultra-intense laser beams. Existing installations and forthcoming high-power laser projects allow testing quantum electrodynamics (QED) as a pillar of the Standard Model in the non-linear regime. Besides XFEL beams, the optical lasers play a key role. Among the latter ones, the ELI-Beam Lines [1] and ELI-Nuclear Physics [2] facilities are widely discussed now, to be seen in the context of many other projects, cf. [3]. For a review on most known upcoming petawatt and exawatt laser projects, see [4] for instance.

When speaking on "elementary QED interaction processes" we have in mind Schwinger pair production, Breit–Wheeler and trident (triple) pair production, and Compton scattering. While ranging from elusive to not much probed to fairly well known, these fundamental phenomena can be considered as corner stones of QED which deserve in-depth investigations in their own right, in particular in the strong-field regime. In the present work we focus on some details of polarization effects in the non-linear Breit–Wheeler (BW) process. Within the Furry picture, the non-linear BW process refers to the decay of a linearly polarized probe photon $\vec{\gamma}'$ with four-momentum $k'(\omega', \mathbf{k}')$ into an electron-positron (e^+e^-) pair while traversing a linearly polarized laser pulse (characterized by the central frequency ω, wave four-vector k and polarization four-vector ε with $\varepsilon \cdot k = 0$, where the dot stands for the scalar product), symbolically $\vec{\gamma}' \to e^-_L + e^+_L$. Here, the label "$L$" points to the laser-dressed $e^\pm$ states. Alternatively, one can characterize the reaction under consideration by $\vec{\gamma}' + \vec{L} \to e^+ + e^-$. Facilities of the probe photon beam polarization for the multi-photon BW process are discussed in [5–7], for instance. Polarized multi-GeV photon beams are in operation worldwide, cf. [8,9].

Various laser polarizations can be accomplished customarily. In the plane-wave approximation, one can further distinguish monochromatic laser beams, formally with an infinitely long duration (that is the infinite-pulse approximation [IPA]), or a pulse of finite duration (that is the finite-pulse approximation [FPA]). In the latter case, the bandwidth effects cause a distribution of frequencies around the central one, as evidenced by the power spectrum of the pulse. The IPA case has been analyzed in depth by Reiss [10] and the Ritus group [11] some time ago, and summarized in a well-known review paper [12]. For completeness, we mention the review papers [13–15], and also recent publications [16–19].

The weak-field BW pair production $\gamma' + \gamma \to e^+ + e^-$ is a threshold process requiring $s > 4m^2$ (where s and m are the square of the total energy in the center of mass system (c.m.s.) and the electron mass, respectively), therefore, for its analysis it is natural to use two dimensionless relativistic and invariant variables. One is the reduced field intensity ξ related to the intensity of background field potential a, and electron charge e, $\xi = ea/m$ [20], and the threshold variable $\zeta \equiv 4m^2/s$ [21] instead of the Mandelstam variable s. The region $\zeta > 1$ automatically selects the sub-threshold multi-photon regime, where the simultaneous participation of a multitude of photons in the laser beam

[a] e-mail: atitov@theor.jinr.ru

via $\gamma' + n\gamma \to e^+ + e^-$ enables the pair production. Instead of ζ, one can equally well use the quantum-nonlinearity parameter κ (known as a Ritus variable), related to ζ by $\kappa = 2\xi/\zeta$.

The SLAC experiment E-144 [22,23] has tested the sub-threshold multi-photon regime with $n > 3$ at $\xi \leq 0.35$ by the trident process $e^- + L \to e^- + e^+ + e^-$ which combines the sub-processes of non-linear Compton back-scattering $e^- + L \to e^- + \gamma'$ and non-linear BW pair production. The envisaged LUXE experiment [24,25] will probe the non-linear BW and trident processes at $\xi > 1$ at the precision level. For further prospects, see [3], in particular w.r.t. FACET-II [26].

Given the present and future experimental research opportunities, the theoretical basis must be developed in more detail. In early works [10–12], it was found that the probability of electron-positron BW pair production depends on the mutual polarization of the probe photon and the laser background field. For example, different probabilities (W) (or cross sections (σ)) have been calculated for the non-linear BW process for mutual polarizations being either perpendicular ($\perp$) or parallel ($\parallel$). In the case of a monochromatic background field and for asymptotically large values $\xi \gg 1$, reference [12] predicts a ratio of $\sigma_\perp/\sigma_\parallel$ equal to 2 and 3/2 for $\kappa \ll 1$ and $\kappa \gg 1$, respectively.

Some definite peculiarities in the differential distributions of positrons depending on the mutually linear polarizations of the laser pulse and probe photon beam at finite values of ξ were considered in [27]. The non-linear BW pair production in short laser pulses was studied in [28] in a wide region of ξ and κ by employing a polarization-operator approach. An exponential decrease of the probability of e^+e^- pair creation with decreasing values of κ was found in the asymptotic region of $\xi \gg 1$, $\kappa \ll 1$. The observed decrease is even stronger than predicted for the constant-cross field, while maintaining the same ratio $W_\perp/W_\parallel$ as in [12].

Another example of e^+e^- BW pair production at relatively high field strengths corresponding to $\xi = 1 \ldots 5$ and the energy of the probe photon $\omega' = 13$ GeV was analyzed in [29] within a semi-classical approach to BW e^+e^- pair production. It was found that, at $\xi = 2$ and $\kappa = 0.3 \ldots 0.4$, the relative probabilities of e^+e^- pair production with different photon polarizations are $W_\perp = 2.04 \ldots 2.05$.

The difference between $\sigma_\perp$ and $\sigma_\parallel$ leads to a finite asymmetry $\mathcal{A} = (\sigma_\perp - \sigma_\parallel)/(\sigma_\perp + \sigma_\parallel)$, which has not yet been subject of an independent research in itself. For example, the asymptotic prediction of [12] at $\xi \gg 1$ leads to variation of the asymmetry in the interval $\mathcal{A} = 1/3$ to $1/5$ for $\kappa \ll 1$ and $\kappa \gg 1$, respectively.

In present work we analyze the asymmetry $\mathcal{A}$ in two regions: (i) at medium-strong ($\xi \leq 1$) and (ii) ultra-strong ($\xi \gg 1$) laser fields, respectively.

In the case of $\xi < 1$, the beam duration (or the number of e.m. field oscillations in the pulse) is important [18,19,28]. Therefore, we analyze the asymmetry as a function of ξ and ζ for different pulse legths, using our formulation developed in [18]. We show that, in this region, the asymmetry may vary within the interval from $\mathcal{A} \simeq 0$ to $\mathcal{A} \simeq 1$ where the cross section can acquire values from $\sigma_\parallel \simeq \sigma_\perp$ to $\sigma_\parallel \ll \sigma_\perp$.

In the case of a strong laser field characterized by $\xi \gg 1$, the dominant contribution to the probability of e^+e^- pair production comes from the central part of the pulse envelope [30]. Therefore, if the number of e.m. field oscillations exceeds unity, the pulse duration becomes insignificant and one can use the constant-crossed field approximation in a wide region of $\zeta\,(\kappa)$ which excludes the appearance of new parameters and assumptions. In both cases, we analyze the dependence of $\mathcal{A}$ on the threshold parameter ζ and on the azimuthal angle of the outgoing electron (positron).

Our paper is organized as follows. In Section 2, for completeness, we recall the laser field model. The deployed basic formulations of the cases $\xi \leq 1$ and $\xi \gg 1$ are presented in Sections 3 and 5. The respective numerical results are discussed in Sections 4 and 6. Our summary is given in Section 7.

2 The background field model

We suppose the external, linearly polarized background (laser pulse) field is determined by the electromagnetic (e.m.) four-potential in the axial gauge $A = (0, \mathbf{A})$ as $\mathbf{E} = -\partial\mathbf{A}/\partial t$:

$$\mathbf{A}(\phi) = f(\phi)\,[\mathbf{a}\cos(\phi)]\,. \tag{1}$$

The quantity $\phi = k \cdot x$ is the invariant phase with four-wave vector $k = (\omega, \mathbf{k})$, obeying the null field property $k^2 = k \cdot k = 0$ implying $\omega = |\mathbf{k}|$, $\mathbf{a} \equiv \mathbf{a}_{(x)}$; $|\mathbf{a}|^2 = a^2$; transversality means $\mathbf{ka} = 0$ in the present gauge. For the sake of definiteness, the envelope function $f(\phi)$ is chosen as hyperbolic secant:

$$f(\phi) = \frac{1}{\cosh\frac{\phi}{\Delta}}. \tag{2}$$

The dimensionless quantity Δ is related to the pulse duration $2\Delta = 2\pi N$, where N has the meaning of the number of cycles in the laser pulse. It is related to the time duration of the pulse $\tau = 2N/\omega$. $N < 1$ means sub-cycle pulses (for the dependence of some observables on the envelope shape, see, e.g. [21]).

For an illustration, Figure 1 exhibits the e.m. potential A of the pulse as a function of invariant phase ϕ for different values of the parameter $N = 0.5$, 1 and 5 shown by solid, dashed and the dash-dotted curves, respectively. These values of N are used in further analysis. The case of $N = 0.5$ corresponds to the sub-cycle pulse.

The cross section of e^+e^--pair production includes a normalization factor N_0 which is related to the average square of the e.m. strength and is expressed through the envelope functions as

$$N_0 = \frac{1}{2\pi}\int\limits_{-\infty}^{\infty} d\phi \left(f^2(\phi) + f'^2(\phi)\right)\cos^2\phi \tag{3}$$

with the asymptotic value $N_0 \approx \Delta/2\pi$ at $\Delta/\pi \gg 1$. We use natural units with $c = \hbar = 1$, $e^2/4\pi = \alpha \approx 1/137.036$.

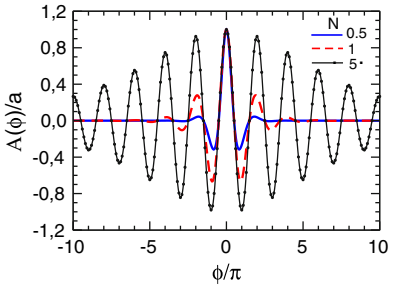

Fig. 1. The electromagnetic potential as a function of invariant phase $\phi = k \cdot x$ for different values of the pulse duration, $N = 1/2$ (blue solid curve), 1 (dashed red curve) and 5 (black dash-dotted curve).

3 Basics of cross section and asymmetry, $\xi \leq 1$

As mentioned above, we consider essentially multi-photon events, where a finite number of laser photons is involved simultaneously in the e^+e^- pair production. This allows for sub-threshold e^+e^- pair production at $s < s_{\rm thr}$ or $\zeta > 1$. In this section we analyze the dependence of cross sections on ζ and on the e.m. field intensity which is described by the reduced field intensity parameter ξ^2 for different mutual polarizations of the incident photon and the laser beam.

The differential cross sections read

$$\frac{d\sigma_i}{d\phi_e} = \frac{2\alpha^2}{m^2\xi\kappa N_0}\int\limits_{\zeta}^{\infty} d\ell\, v(\ell)\int\limits_{-1}^{1} d\cos\theta_e\, w_i(\ell), \qquad (4)$$

where $i = \perp, \parallel$, ℓ is an auxiliary continuous variable, $w_i(\ell)$ denotes the partial probability of the process process. The azimuthal angle of the outgoing electron, ϕ_e, is defined as $\cos\phi_e = \mathbf{a}_x\mathbf{p}_e/a|\mathbf{p}_e|$. It is related to the azimuthal angle of the positron by $\phi_{e^+} = \phi_e + \pi$. Furthermore, θ_e is the polar angle of the outgoing electron, v is the electron (positron) velocity in the center of mass system (c.m.s.).

The lower limit of the integral over the variable ℓ is the threshold parameter ζ.

The region of $\zeta < 1$ corresponds to the above-threshold e^+e^- pair production, while the region of $\zeta > 1$ is for the sub-threshold pair production enabled by multi-photon and bandwidth effects. We keep our notation in [18] and denote by $k(\omega, \mathbf{k})$, $k'(\omega', \mathbf{k}')$, $p(E, \mathbf{p})$ and $p'(E', \mathbf{p}')$ the four-momenta of the background (laser) field, the incoming probe photon, the outgoing positron and the outgoing electron, respectively. The important variables s, v and u are determined by $s = 2k\cdot k' = 2(\omega'\omega - \mathbf{k}'\mathbf{k})$ (with $\mathbf{k}'\mathbf{k} = -\omega'\omega$ for head-on geometry), $v^2 = (\ell s - 4m^2)/\ell s$, $u \equiv (k'\cdot k)^2/\left(4(k\cdot p)(k\cdot p')\right) = 1/(1 - v^2\cos^2\theta_e)$. The Ritus variable $\kappa = \xi(k\cdot k')/m^2$, is related to ζ by $\kappa = 2\xi/\zeta$. Note the identity

$$v(\ell)\int\limits_{-1}^{1} d\cos\theta_e = \int\limits_{1}^{u_\ell}\frac{du}{u\sqrt{u(u-1)}} \qquad (5)$$

with $u_\ell = \ell/\zeta$. The normalization factor N_0 is given by equation (3).

In cases, where the incident probe photon polarization plane is parallel ($\parallel$) or perpendicular ($\perp$) to the laser beam polarization, the partial probabilities $w_i(\ell)$ have the following form:

$$\begin{aligned} w_\parallel(\ell) &= \xi^2(u-1)\left(|\widetilde{A}_1(\ell)|^2 - \mathrm{Re}[\widetilde{A}_0(\ell)\widetilde{A}_2^*(\ell)\right) \\ &\quad + (1+\tau^2)|\widetilde{A}_0(\ell)|^2, \\ w_\perp(\ell) &= \xi^2\, u\,\left(\widetilde{A}_1(\ell)|^2 - \mathrm{Re}[\widetilde{A}_0(\ell)\widetilde{A}_2^*(\ell)\right) - \tau^2|\widetilde{A}_0(\ell)|^2, \end{aligned} \qquad (6)$$

where $\tau^2 = (u/u_\ell - 1)\sin^2\phi_e$. The basic functions $\widetilde{A}_m$ introduced in [18] are analogs of the well known IPA basis functions $A_m(n)$ in [12]:

$$\widetilde{A}_m(\ell) = \frac{1}{2\pi}\int\limits_{-\infty}^{\infty} d\phi\, f^m(\phi)\cos^m(\phi+\tilde{\phi})\,\mathrm{e}^{i\ell\phi - i\mathcal{P}^{(Lin)}(\phi)} \qquad (7)$$

with

$$\mathcal{P}^{(lin)}(\phi) = \tilde{\alpha}(\phi) - \tilde{\beta}(\phi), \qquad (8)$$

$$\tilde{\alpha}(\phi) = \alpha\int\limits_{-\infty}^{\phi} d\phi' f(\phi')\cos\phi', \qquad (9)$$

$$\tilde{\beta}(\phi) = 4\beta\int\limits_{-\infty}^{\phi} d\phi' f^2(\phi')\cos^2\phi',$$

$$\alpha = z\cos\phi_e,\ \beta = \frac{\xi^3 u}{2\kappa},\ z = \frac{4\xi^2 u}{\kappa}\sqrt{\frac{u_\ell}{u} - 1}. \qquad (10)$$

The integrand of the function $\widetilde{A}_0(\ell)$ in equation (7) does not contain the envelope function $f(\phi)$ and is, therefore, divergent. It is regularized using the prescription of [31,32] which leads to identity

$$\ell\widetilde{A}_0(\ell) = \alpha\widetilde{A}_1(\ell) - 4\beta\widetilde{A}_2(\ell). \qquad (11)$$

The definitions in equation (6) resemble corresponding IPA expressions, i.e. for a monochromatic background field one has [12]

$$\begin{aligned} w_{\parallel n} &= \xi^2(u-1)\,(A_1^2 - A_0A_2) + (1+\tau^2)\,A_0^2, \\ w_{\perp n} &= \xi^2\,u\,(A_1^2 - A_0A_2) - \tau^2\,A_0^2, \end{aligned} \qquad (12)$$

which can be obtained by replacing the basis functions $\widetilde{A}_m(\ell) \to A_m \equiv A_m(n\alpha\beta)$ determined as

$$A_m(n\alpha\beta) = \frac{1}{2\pi}\int\limits_{-\pi}^{\pi} d\phi\cos^m(\phi)\,\mathrm{e}^{in\phi - i\alpha\sin\phi + i\beta\sin 2\phi} \qquad (13)$$

with $z^2 \to z^2(1+\xi^2/2)$, $\tau^2 \to \tau^2(1+\xi^2/2)$, $\zeta \to \zeta(1+\xi^2/2)$, and with obvious substitutions $\ell \to n$ in (4). Thus, the corresponding differential cross sections read

$$\frac{d\sigma_i^{IPA}}{d\phi_e} = \frac{2\alpha^2}{m^2\xi\kappa N_0}\int\limits_{1}^{\infty}\frac{du}{u^{3/2}\sqrt{u-1}}\sum_{n=n_{\min}}^{\infty} w_{in}, \qquad (14)$$

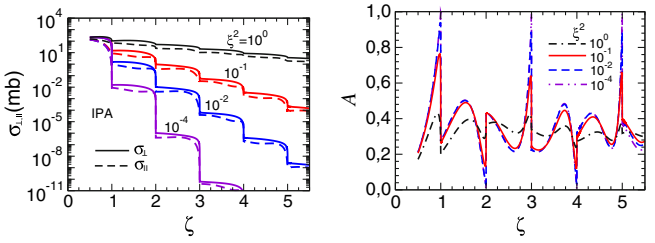

Fig. 2. Results for a monochromatic laser beam, i.e. an infinitely long pulse (IPA). Left panel: cross sections $\sigma_\perp$ (solid curves) and $\sigma_\parallel$ (dashed curves) as a function of the threshold parameter ζ for $\xi^2 = 10^0$, 10^{-1}, 10^{-2} and 10^{-4}. Right panel: asymmetry as a function of ζ.

with $N_0 = 1/2$. The limit $n_{\min}$ is determined as through integer part (Int) of $n_{\min} = \mathrm{Int}\left((4m^2(1+\xi^2/2))/s\right) + 1$, see [12,18] for details.

The cross section for an unpolarized incoming probe photon is given by equation (4) with

$$w(\ell) = \frac{1}{2}(w_\perp(\ell) + w_\parallel(\ell)). \tag{15}$$

The difference in $w_\perp$ and $w_\parallel$ allows to introduce the asymmetry for the total cross section, integrated over ϕ_e, by

$$\mathcal{A} = \frac{\sigma_\perp - \sigma_\parallel}{\sigma_\perp + \sigma_\parallel}, \tag{16}$$

as a function of ζ, as well as the asymmetry of a function of ϕ_e at fixed ζ by

$$\mathcal{A}(\phi_e) = \frac{d\sigma_\perp/d\phi_e - d\sigma_\parallel/d\phi_e}{d\sigma_\perp/d\phi_e + d\sigma_\parallel/d\phi_e}. \tag{17}$$

4 Numerical results, $\xi \leq 1$

Below we present our numerical results for the cross sections and asymmetries for the the monochromatic laser beam (IPA) and for short and ultra-short (sub-cycle) pulses (FPA).

4.1 Infinite pulse (IPA)

The cross sections as a function of the threshold parameter ζ are exhibited in the left panel of Figure 2 for $\xi^2 = 10^0$, 10^{-1}, 10^{-2} and 10^{-4}. The cross sections $\sigma_\perp$ and $\sigma_\parallel$ are depicted by solid and dashed curves, respectively.

One can see a step-like behavior of the cross sections, where each new step with ζ close to its integer value n_ζ corresponds to opening a new channel with the number of simultaneously participating photons exceeding n_ζ. The step height is proportional to ξ^{-2}. At $\xi^2 = 1$, the stepwise behavior practically disappears, and the cross sections show an almost smooth decrease with increasing ζ.

The asymmetry defined in equation (16) as a function of the threshold parameter ζ is exhibited in Figure 2, right panel. For a weak field strength, $\xi^2 \ll 1$, the asymmetry exhibits sharp peaks and dips in the vicinity $\zeta \simeq 2m+1-\epsilon$ and $\zeta \simeq 2m - \epsilon$ with $m = 0, 1, 2\ldots$ and $\epsilon \ll 1$, respectively. The height of the peaks (the depth of the dips) reaches a value of $\mathcal{A} \simeq 1\,(0)$ at $\xi^2 \leq 10^{-4}$ and decreases (increases) with increasing values of ξ^2.

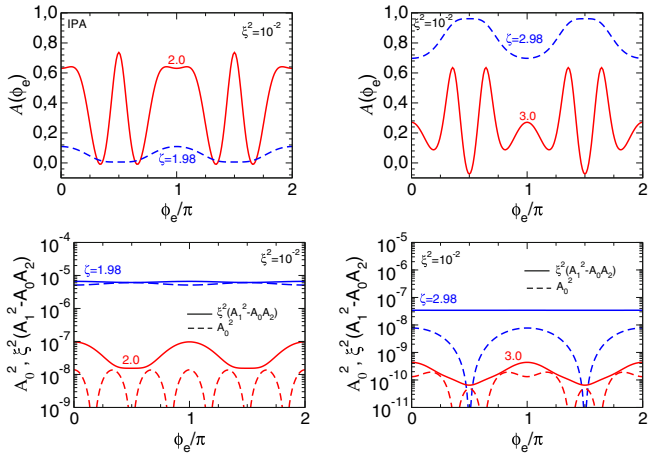

Fig. 3. The asymmetry and combinations of A_m as a function of ϕ_e for an infinitely long pulse (IPA) for $\xi^2 = 10^{-2}$. The upper and top panels are for asymmetries $\mathcal{A}$ and functions $f_1 = \xi^2(A_1^2 - A_1A_2)$ and $f_2 = A_0^2$, respectively; the left and right panels correspond to $\zeta = 2$ and 3, respectively. The functions f_1 and f_2 are shown by solid and dashed curves, respectively.

Sharp peak or dip positions correspond to the cases where $\sigma_\perp \gg \sigma_\parallel$ or $\sigma_\perp \simeq \sigma_\parallel$, respectively, and reflect the properties of the basic functions $A_m(n)$. Note that the non-monotonic ζ dependence of asymmetry is determined by the numerator in the expression (16).

In the here considered case of IPA one has

$$\begin{aligned}\mathcal{A}(\phi_e) &\propto \sum_{n=n_{\min}}^{\infty} \int_{-1}^{1} v d\cos\theta_e \\ &\times \left(\xi^2\left(A_1^2 - A_0A_2\right) - \left(1+2\tau^2\right)A_0^2\right) \\ &\sim \xi^2\left(A_1^2 - A_0A_2\right) - A_0^2\,|_{n=n_{\min},\theta=\pi/2,\tau=0},\end{aligned} \tag{18}$$

neglecting a small, slowly varying variable τ^2, and taken integrand at $\cos\theta = 0$, $n = n_{\min}$ where the integral reaches its maximum value.

For an illustration, Figure 3 exhibits the asymmetry $\mathcal{A}(\phi_e)$ and the combination of the functions $f_1 = \xi^2(A_1^2 - A_0A_2)$ and $f_2 = A_0^2$, which are depicted in the top and bottom panels, respectively. The dependence on the azimuthal angle in the vicinity of $\zeta = 2$ and 3, is shown in the left and right panels, respectively. When $\zeta = 2 - \epsilon$, then $f_1 \simeq f_2$, which leads to a small asymmetry and manifests itself in a dip in the right panel of Figure 2. For $\zeta = 3 - \epsilon$, one gets $f_1 \gg f_2$ and, as a result, the asymmetry exhibits a sharp peak in the right panel of Figure 2.

Finally, we conclude that in the region under consideration, $\xi^2 \leq 1$ and $\zeta \leq 5$, the asymmetry shows sharp peaks and dips in such a way that for $\xi^2 \leq 10^{-4}$ the asymmetry varies in the range $0 \lesssim \mathcal{A} \lesssim 1$. With increasing values of

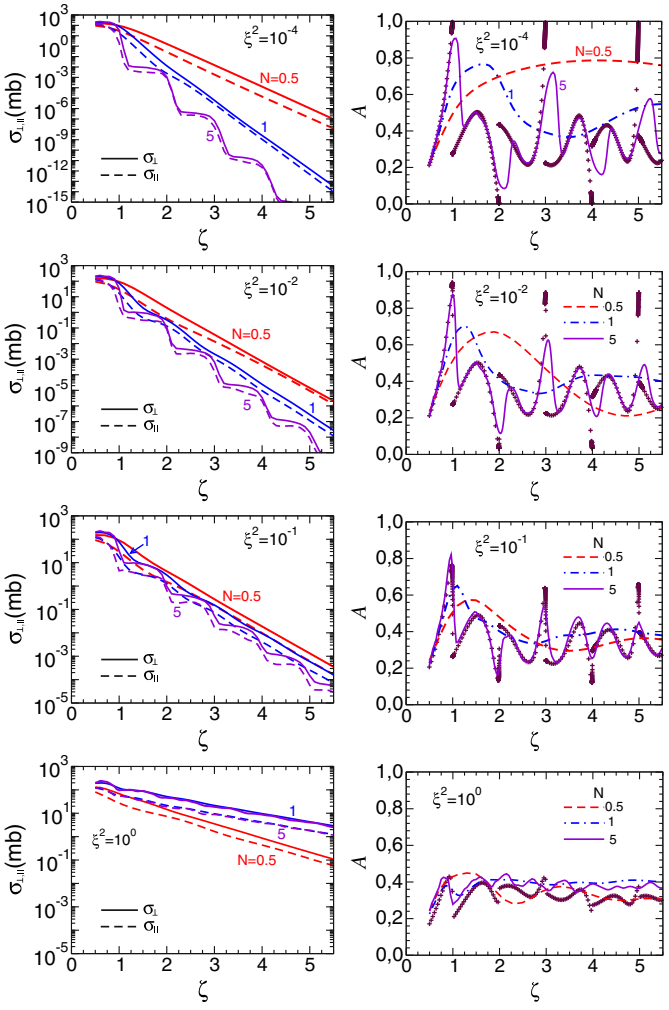

Fig. 4. Left panels: total cross sections of the non-linear BW e^+e^- pair production as a function of the threshold parameter ζ for finite pulses with $N = 0.5$, 1 and 5. The results for $\xi^2 = 10^{-4}$, 10^{-2}, 10^{-1}, and 10^0 are displayed sequentially from the top to bottom panels. The solid and dashed curves are for $\sigma_\perp$ and $\sigma_\parallel$, respectively. Right panels: asymmetry as a function of ζ for different values of ξ^2 and N. The dashed, dot-dashed and solid curves are for $N = 0.5$, 1 and 5, respectively. Crosses are for the infinite pulse (IPA) prediction.

ξ^2, the range of the variation decreases significantly. At $\xi^2 = 1$, the asymmetry varies in the range $0.2 \ldots 0.4$ with average value ≈ 0.33.

4.2 Finite pulse (FPA)

Our results for non-linear Breit–Wheeler e^+e^- pair production as a function of the threshold parameter ζ for finite pulses (FPA) with different pulse lengths (characterized by N) and field intensity ξ^2 are exhibited in Figure 4.

The total cross sections $\sigma_\perp$ and $\sigma_\parallel$ as a function of ζ for $\xi^2 = 10^{-4}$, 10^{-2}, 10^{-1}, and 10^0 are displayed sequentially from the top to bottom panels in Figure 4 (left). The solid and dashed curves are for $\sigma_\perp$ and $\sigma_\parallel$, respectively.

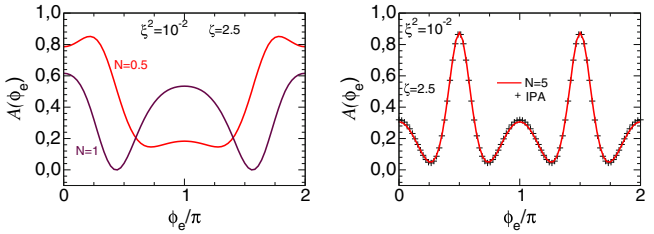

Fig. 5. The asymmetry as a function of ϕ_e for finite pulses characterized by $N = 0.5$, 1 (left panel) and $N = 5$ (right panel) at $\zeta = 2.5$ and $\xi^2 = 10^{-2}$. The crosses in the right panel are for the IPA case.

In the case of $N = 5$ and $\xi^2 \lesssim 10^{-1}$, the cross sections exhibit a step-like structure with steps near the integer values of ζ, similar to the IPA prediction shown in Figure 2. The height of the steps $\propto \xi^{-2}$. At $\xi^2 = 1$, the step-wise structure of the cross sections goes into an almost monotonic decrease with increasing ζ. The cross sections for $N = 1$ and 5 are close to each other, i.e. the result becomes insensitive to the pulse duration.

In the cases of short ($N = 1$) and very short (sub-cycle, $N = 0.5$) pulses, the cross sections exhibit a monotonic exponential decrease with increasing ζ.

The difference between $\sigma_\perp$ and $\sigma_\parallel$ leads to a finite asymmetry, displayed in the right panels of Figure 4. For convenience, the prediction for the IPA case is shown by crosses. Consider first the case of a weak field, i.e. an intensity referring to $\xi^2 \lesssim 10^{-1}$. At a relatively large pulse width with $N \geq 5$, the asymmetry resembles qualitatively IPA result (cf. Fig. 2, right) with some peaks and dips. Their positions are close to that of the IPA case.

At sub-cycle and short pulses with $N = 0.5$ and 1, respectively, the asymmetries exhibit smooth non-monotonic behavior without sharp peaks and dips.

Let us analyze the asymmetry as a function of the azimuthal angle ϕ_e. First, we consider the case of ζ being in the interval between the two nearest integer values, i.e. away from the values for which IPA predicts sharp peaks/dips.

Our result for $\zeta = 2.5$ and $\xi^2 = 10^{-2}$ is depicted in Figure 5. Predictions for very short pulses with $N \leq 1$ and short pulses with $N \geq 5$ are different, therefore, they are shown separately.

For pulse with $N = 0.5$, the asymmetry is quite a large at $\phi_e = 0$ ($\mathcal{A}(0) \simeq 0.8$), increases toward a local maximum at $\phi \simeq \pi/4$, and then decreases toward a minimum at $\phi_e = \pi/2$. (Note that the asymmetry is symmetric under the substitution $\phi_e \to 2\pi - \phi_e$.) For the short pulse with $N = 1$, the asymmetry has a maximum at $\phi_e = 0$, then it decreases up to zero at $\phi_e/\pi \simeq 0.44$ and has a maximum at $\phi_e = \pi$.

In case of a pulse with $N = 5$, the asymmetry exhibits local maxima at $\phi_e = 0\,\pi/2$, π and minima at $\pi/4$, $3\pi/4$. The result for the finite pulse coincides practically with the prediction for the IPA case, shown by crosses.

For completeness, in Figure 6 we also present results for the asymmetry in the vicinity of integer values of $\zeta = 2$. The asymmetries for $N = 0.5$, 1 and $N = 5$ are shown in

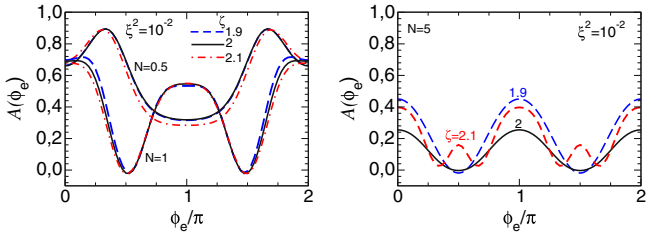

Fig. 6. The asymmetry as a function of ϕ_e for finite pulses with $N = 0.5$, 1 (left panels) and $N = 5$ (right panels) and $\zeta = 1.9$, 2, 2.1 at $\xi^2 = 10^{-2}$.

the left and right panels, respectively. In our calculations, we choose $\zeta = 1.9$, 2, and 2.1 at $\xi^2 = 10^{-2}$. In the case of short pulses with $N \leq 1$, the result is similar to that shown in Figure 6 (left panel) and, within the chosen interval, is practically independent of ζ. For $N \geq 5$, the model predicts clear maxima at $\phi_e = 0$, π. An additional bump occurs at $\phi_e = \pi/2$ and $\zeta = 2.1$, but its height is much smaller than that predicted for $\zeta = 2.5$ (cf. Fig. 5 (right panel)).

5 Cross sections and asymmetry in ultra-intense fields, $\xi \gg 1$

At large values of $\xi \gg 1$, the main contribution to the e^+e^- pair production comes from the central part of envelope, the final result is not sensitive to the envelope structure [30], and for calculation of the partial probabilities one can use the IPA formalism with replacing the summation $\sum_n$ in equation (14) by the integration $\int d\ell$. The total cross section reads

$$\frac{d\sigma_i}{d\phi_e} = \frac{2\alpha^2}{m^2\xi\kappa N_0}\int_0^{2\pi} d\phi \int_1^{\infty} \frac{du}{u^{3/2}\sqrt{u-1}} \int_{\ell_{\min}}^{\infty} d\ell\, w_{i\ell}, \quad (19)$$

where $\phi = \phi_e$ and $\ell_{\min} = 4m^2(1+\xi^2/2)u/s$, and $N_0 = 1/2$. The corresponding formalism was developed by Nikishov and Ritus [11,12]. For completeness and easy reference, we provide in this section the most important expressions of their approach, necessary for the subsequent analysis.

The continuous variable ℓ is expressed in terms of the auxiliary variables ρ and τ via

$$\ell = \frac{2\xi^2 u}{\kappa}\left(\rho^2 + \frac{\tau^2}{\xi^2}\right) + \ell_{\min}, \quad (20)$$

where

$$\rho^2 = \frac{1}{\xi^2}\left(1+\frac{1}{2}\xi^2\right)\left(\frac{u_\ell}{u}-1\right)\cos^2\phi,$$
$$\tau^2 = \left(1+\frac{1}{2}\xi^2\right)\left(\frac{u_\ell}{u}-1\right)\sin^2\phi, \quad (21)$$

with $\ell_{\min} \equiv \ell_0 = 2m^2(1+\frac{1}{2}\xi^2)/(k\cdot k') = 2\xi(1+\xi^2/2)/\kappa$ and $u_\ell = \ell/\ell_0$. The variables ρ, τ and ϕ allow to perform a useful transformation

$$\int_0^{2\pi} d\phi \int_{\ell_{\min}}^{\infty} d\ell = \frac{4\xi^2 u}{\kappa}\int_{-\infty}^{\infty} d\rho \int_{-\infty}^{\infty} d\tau. \quad (22)$$

Further, for large ℓ the arguments α and β in the basic functions $A_m(\ell\alpha\beta)$ in equation (13) are also large and, therefore, the bi-linear combinations of A_0^2 and $A_1^2 - A_0A_2$ in (12) can be replaced by asymptotic expressions:

$$A_0^2 = \frac{2\sigma}{\pi^2\xi^2 y\,\sin^2\psi}\Phi^2(y)(1+\cos 2\eta)$$
$$A_1^2 - A_0A_2 = \frac{2\sigma^2}{\pi^2\xi^4 y^2\,\sin^2\psi}\left(y\,\Phi^2(y) + \Phi'^2(y)\right. \quad (23)$$
$$\left. + \left(y\,\Phi^2(y) + \Phi'^2(y)\right)\cos 2\eta\right), \quad (24)$$

where $\Phi(y)$ and $\Phi'(y)$ denote the Airy function and its derivative, respectively. The variables ψ, σ, and η are associated with the variables ℓ, u, ρ, and τ as

$$\cos\psi = \rho,\ \sigma = 1+\tau^2,\ y = \sigma\left(\frac{2u}{\kappa\sin\psi}\right)^{\frac{2}{3}},$$
$$\eta = \ell\left(\psi - \frac{\sin 2\psi}{2(1+2\cos^2\psi)}\right). \quad (25)$$

By making use of equations (23)–(25) and discarding highly-oscillating terms proportional to $\cos 2\eta$, one can obtain the final expressions for σ_i $(i = \perp, \parallel)$

$$\sigma_{i\,\infty} = \frac{32\alpha^2}{\pi^2\,\xi\kappa\,m^2}\int_0^{\pi} d\psi \int_0^{\infty} \frac{dt}{(t^2+1)^{\frac{3}{2}}} \int_{-\infty}^{\infty} d\tau w_i \quad (26)$$

with $t = \sqrt{u-1}$ and

$$w_{\perp\,\infty} = a\left(u\,F_1 - \tau^2 F_2\right),$$
$$w_{\parallel\,\infty} = a\left((u-1)\,F_1 + (1+\tau^2)F_2\right), \quad (27)$$
$$F_1 = b\left(y\,\Phi^2(y) + \Phi(y)'^2\right),\ F_2 = \Phi^2(y),$$
$$a = a_0^{\frac{1}{3}},\ b = a_0^{-\frac{2}{3}},\ a_0 = \frac{2u}{\kappa\sin\psi}. \quad (28)$$

The difference between $\sigma_\perp$ and $\sigma_\parallel$ in equations (26), (27) leads to the asymmetry

$$\mathcal{A}_\infty = \frac{\sigma_{\perp\,\infty} - \sigma_{\parallel\,\infty}}{\sigma_{\perp\,\infty} + \sigma_{\parallel\,\infty}}. \quad (29)$$

In the limit of extremely large values of $\zeta \gg 2\xi$ (small values of $\kappa \ll 1$) and small values of $\zeta \gg 2\xi$ (large values

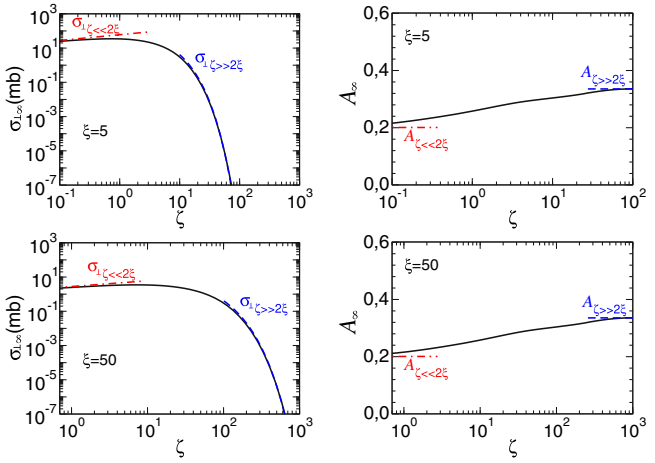

Fig. 7. The left and right panels are for the total cross section $\sigma_{\perp\infty}$ and asymmetry $\mathcal{A}_\infty$ as a function of ζ. The dashed and dot-dashed curves are for the asymptotic expressions equations (30) and (31), respectively. The top and bottom panels are for $\xi = 5$ and 50, respectively.

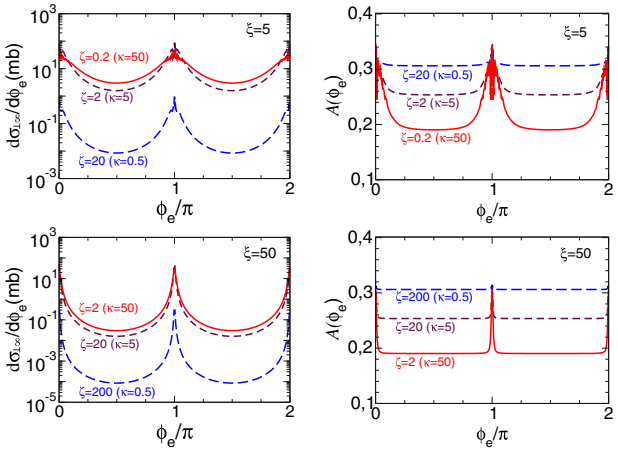

Fig. 8. The left and right panels are for the differential cross sections $d\sigma_{\perp\infty}/d\phi_e$ and the asymmetry $\mathcal{A}_\infty(\phi_e)$ as a function of the azimuthal angle ϕ_e for different values of $\zeta\,(\kappa)$. The top and bottom panels are for $\xi = 5$ and 50, respectively.

of $\kappa \gg 1$), the cross sections take the asymptotic forms

$$\begin{aligned}
&\zeta \gg 2\xi, \ \text{or} \ \ \kappa \ll 1 \\
\sigma_{\perp\infty} &= C_\zeta\, \zeta^{-\frac{1}{2}} e^{-\frac{4}{3}\frac{\zeta}{\xi}} = C_\kappa\, \kappa^{\frac{1}{2}} e^{-\frac{8}{3\kappa}}, \ \ \sigma_{\parallel\infty} = \frac{1}{2}\sigma_{\perp\infty}, \\
C_\zeta &= 3\sqrt{\frac{\pi}{\xi}}\frac{\alpha^2}{m^2}, \qquad C_\kappa = 3\sqrt{\frac{\pi}{2}}\frac{\alpha^2}{m^2\xi}, \qquad (30) \\
&\zeta \ll 2\xi \ \text{or} \ \ \kappa \gg 1, \\
\sigma_{\perp\infty} &= D_\zeta\, \zeta^{\frac{1}{3}}, \ = D_\kappa\, \kappa^{-\frac{1}{3}}, \ \ \sigma_{\parallel\infty} = \frac{2}{3}\sigma_{\perp\infty}, \\
D_\zeta &= \frac{3^{\frac{14}{3}}\Gamma^7(\frac{3}{2})\,\alpha^2}{7\pi^3\xi^{\frac{4}{3}}m^2}, \qquad D_\kappa = \frac{2^{\frac{1}{3}}3^{\frac{14}{3}}\Gamma^7(\frac{3}{2})\,\alpha^2}{7\pi^3\xi m^2}. \qquad (31)
\end{aligned}$$

This leads to the asymptotic expressions for the asymmetry

$$\mathcal{A}_{\zeta\gg 2\xi} = \frac{1}{3}, \qquad \mathcal{A}_{\zeta\ll 2\xi} = \frac{1}{5}. \qquad (32)$$

6 Numerical results, $\xi \gg 1$

The total cross sections $\sigma_{\perp\infty}$ and the asymmetry $\mathcal{A}_\infty$ are exhibited in Figure 7 in the left and right panels, respectively. Results for $\xi = 5$ and 50 are displayed in the top and bottom panels, respectively. The dashed and dot-dashed curves are for the asymptotic expressions equations (30) and (31), respectively. At small values of ζ, the cross sections increase slightly from their asymptotic values and then rapidly decrease with increasing ζ, being nevertheless finite, even at very large values of $\zeta \gg 1$.

The asymmetry monotonically increases with increasing values of ζ, being in the range of its asymptotic values

$$0.2 \geq A_\infty \geq \frac{1}{3}. \qquad (33)$$

Using the identity

$$\cos\psi = \frac{\tau}{\xi}\cot\phi, \qquad (34)$$

one can find expressions for the azimuthal angle-differential cross section

$$\frac{d\sigma_{i\,\infty}}{d\phi} = \frac{32\alpha^2}{\pi^2\,\xi^2\kappa\,m^2\sin^2\phi}\int_0^\infty \frac{dt}{(t^2+1)^{\frac{3}{2}}}\int_{-\infty}^{\infty}\frac{\tau d\tau}{\sin\psi}w_i, \qquad (35)$$

and the azimuthal angle asymmetry

$$\mathcal{A}_\infty(\phi) = \frac{d\sigma_{\perp\infty}/d\phi - d\sigma_{\parallel\infty}/d\phi}{d\sigma_{\perp\infty}/d\phi + d\sigma_{\parallel\infty}/d\phi}. \qquad (36)$$

The differential cross sections $d\sigma_{\perp\infty}/d\phi_e$ and asymmetry $\mathcal{A}_\infty(\phi_e)$ as a function of the azimuthal angle ϕ_e for different values of $\zeta\,(\kappa)$ are depicted in Figure 8 in the left and right panels, respectively. The cross sections exhibit a deep minimum at $\phi_e = \pi/2$ and sharp maxima at $\phi_e = 0, \pi$, respectively. The cross sections decrease with increasing values of ζ.

The asymmetry has sharp peaks at $\phi_e = 0, \pi$. The height of the peaks increases with decreasing ζ. The value of asymmetry in the region $0 < \phi_e < \pi$ is consistent with asymptotic prediction equation (32).

7 Summary

In summary we have performed an analysis of the asymmetry of e^+e^- pair production by the non-linear BW process for different mutual orientations of the polarization vectors of a linearly polarized initial probe photon and the linearly polarized laser pulse for low ($\xi \leq 1$) and high ($\xi \gg 1$) laser field intensities. In particular, we examined the asymmetry caused by the difference of $\sigma_\perp$ and $\sigma_\parallel$. We have analyzed the asymmetry for both the total cross sections as a function of the threshold parameter ζ and the

differential cross sections as a function of the azimuthal electron angle ϕ_e for fixed values of ζ. Our results can be summarized as follows.

(1) Weak field intensity with $\xi \leq 1$:
   (i) the cross sections $\sigma_\perp$ and $\sigma_\parallel$ decrease fast with increasing threshold variable ζ. The cross sections are sensitive to the pulse duration. Thus, at relatively large laser pulse duration, $N \geq 5$, $\sigma_{\perp,\parallel}$ exhibit a step-like behavior, similar to the prediction for an infinite pulse. The height of steps is $\propto \xi^{-2}$. In case of short and sub-cycle pulses with $N \leq 1$, the cross sections decrease monotonically with increasing ζ. At $\xi = 1$ we found a weak dependence on the pulse duration for $N \geq 1$.
   (ii) The difference between $\sigma_\perp$ and $\sigma_\parallel$ generates a specific asymmetry, both for monochromatic laser beams (IPA) and pulses of finite duration (FPA). In IPA it has sharp peaks and dips at integer odd and even values of ζ, respectively. That is a consequence of properties of the corresponding basic functions A_m. In FPA and for pulses with $N \geq 5$, the asymmetry also exhibits a non-monotonic behavior with pronounced peaks and dips. Their positions resemble that of IPA. At small values of N, $N \leq 1$, the asymmetry is a smooth monotonic function of ζ.
   (iii) The azimuthal angle dependence of the asymmetries displays smooth non-monotonic distributions with specific maxima and minima which are determined by the pulse duration and the threshold parameter ζ.

(2) High laser field intensity with $\xi \gg 1$:
   (i) the cross sections decrease monotonically with increasing values of ζ (or decreasing κ). At asymptotically small and large ζ they coincide with the asymptotic prediction of [12].
   (ii) The asymmetry increases smoothly with increasing ζ from 1/5 to 1/3 for $\zeta \ll 1$ and $\zeta \gg 1$, respectively.
   (iii) The azimuthal angle distribution exhibits sharp peaks at $\phi_e = 0, \pi$. The height of the peaks increases with decreasing values of ζ.

Our theoretical predictions in a wide region of field intensities may be used as a unique and powerful input for the design of forthcoming experiments in the near future and corresponding high-precision experimental studies of the various aspects of multi-photon dynamics in non-linear QED processes.

The authors gratefully acknowledge the collaboration with D. Seipt, T. Nousch, T. Heinzl, and useful discussions with A. Ilderton, K. Krajewska, M. Marklund, C. Müller, and R. Schützhold. A. Ringwald is thanked for explanations w.r.t. LUXE. The work is supported by R. Sauerbrey and T. E. Cowan w.r.t. the study of fundamental QED processes for HIBEF.

Author contribution statement

The authors have contributed equally to the publication, being variously involved in the conceptual outline, software development and numerical evaluations.

Note added in proof: After completion of our work we became aware of a paper by D. Seipt and B. King in [33] "Spin and polarisation dependent LCFA rates for nonlinear Compton and Breit-Wheeler processes", where further polarization effects are studied.

References

1. Extreme Light Infrastructure – Beam-Lines (ELI-Beams), https://www.eli-beams.eu/
2. Extreme Light Infrastructure – Nuclear Physics (ELI-NP), https://www.eli-np.ro/
3. S. Meuren et al., On seminal HEDP research opportunities enabled by colocating multi-petawatt laser with high-density electron beams, arXiv:2002.10051 [physics.plasm-ph] (2020)
4. C.N. Danson et al., High Power Laser Sci. Eng. **7**, e54 (2019)
5. Y.F. Li, R. Shaisultanov, Y.Y. Chen, F. Wan, K.Z. Hatsagortsyan, C.H. Keitel, J.X. Li, Phys. Rev. Lett. **124**, 014801 (2020)
6. T.G. Blackburn, M. Marklund, Plasma Phys. Control. Fusion **60**, 054009 (2018)
7. F. Wan, Y. Wang, R.-T. Guo, Y.-Y. Chen, R. Shaisultanov, Z.-F. Xu, K.Z. Hatsagortsyan, C.H. Keitel, J.-X. Li, Phys. Rev. Res. **2**, 032049 (2020)
8. P. Ambrozewicz et al., Phys. Lett. B **797**, 134884 (2019)
9. S. Adhikari et al., The GlueX Beamline and Detector, arXiv:2005.14272 [physics.ins-det] (2020)
10. H.R. Reiss, J. Math. Phys. **3**, 59 (1962)
11. A.I. Nikishov, V.I. Ritus, Sov. Phys. JETP. **19**, 529 (1964)
12. V.I. Ritus, J. Sov. Laser Res. (United States) **6:5**, 497 (1985)
13. G.A. Mourou, T. Tajima, S.V. Bulanov, Rev. Mod. Phys. **78**, 309 (2006)
14. A.D. Piazza, C. Müller, K.Z. Hatsagortsyan, C.H. Keitel, Rev. Mod. Phys. **84**, 1177 (2012)
15. N.B. Narozhny, A.M. Fedotov, Contempt. Phys. **56**, 249 (2015)
16. K. Homma, D. Habs, G. Mourou, H. Ruhl, T. Tajima, Prog. Theor. Phys. Suppl. **193**, 224 (2012)
17. A. Di Piazza, M. Tamburini, S. Meuren, C.H. Keitel, Phys. Rev. A **99**, 022125 (2019)
18. A.I. Titov, A. Otto, B. Kämpfer, Eur. Phys. J. D **74**, 39 (2020)
19. T. Heinzl, B. King, A.J. MacLeod, The locally monochromatic approximation to QED in intense laser fields, arXiv:2004.13035 [hep-ph] (2020)
20. V.B. Berestetskii, E.M. Lifshitz, L.P. Pitaevskii, Quantum electrodynamics, 2nd edition, in *Course of Theoretical Physics* (Pergamon, Oxford, New York, 1982), Vol. 4
21. A.I. Titov, B. Kämpfer, A. Hosaka, H. Takabe, Phys. Part. Nucl. **47**, 456 (2016)
22. D.L. Burke et al., Phys. Rev. Lett. **79**, 1626 (1997)
23. C. Bamber et al., Phys. Rev. D. **60**, 092004 (1999)
24. M. Altarelli et al., Summary of strong-field QED Workshop, arXiv:1905.00059 [hep-ex] (2019)
25. H. Abramowicz et al., Letter of intent for the LUXE Experiment, arXiv:1909.00860 [physics.ins-det] (2019)

26. S. Meuren, FACET-II SFQED Collaboration, Probing Strong-field QED at FACET-II, Experimental proposal (approved as E-320), unpublished, 2018
27. K. Krajewska, J.Z. Kaminski, Phys. Rev. A **86**, 052104 (2012)
28. S. Meuren, K.Z. Hatsagortsyan, C.H. Keitel, A. Di Piazza, Phys. Rev. D **91**, 013009 (2015)
29. T.N. Wistisen, Phys. Rev. D **101**, 076017 (2020)
30. A.I. Titov, B. Kämpfer, H. Takabe, A. Hosaka, Phys. Rev. A **87**, 042106 (2013)
31. M. Boca, V. Florescu, Phys. Rev. A **80**, 053403 (2009)
32. M. Boca, V. Florescu, Phys. Rev. A **81**, 039901 (2010)
33. D. Seipt, B. King, arXiv:2007.11837 [physics.plasm-ph] (2020)